ACS Catalysis

Research Article

Cite This: ACS Catal. 2019, 9, 1396−1407

pubs.acs.org/acscatalysis

The Catalytic Cycle of Water Oxidation in Crystallized Photosystem II Complexes: Performance and Requirements for Formation of Intermediates

Gennady Ananyev,[†,‡] Shatabdi Roy-Chowdhury,[§] Colin Gates,[†,‡] Petra Fromme,[§] and G. Charles Dismukes*[,†,‡]

[†]Department of Chemistry & Chemical Biology and [‡]Waksman Institute of Microbiology, Rutgers University, Piscataway, New Jersey 08854, United States

[§]Biodesign Center for Applied Structural Discovery, The Biodesign Institute and School of Molecular Sciences Arizona State University, Tempe, Arizona 85287, United States

Supporting Information

ABSTRACT: Crystals of photosystem II (PSII) contain the most homogeneous copies of the water-oxidizing reaction center where O_2 is evolved (WOC). However, few functional studies of PSII operation in crystals have been carried out, despite their widespread use in structural studies. Here we apply oximetric methods to determine the quantum efficiency and lifetimes of intermediates of the WOC cycle as a function of added electron acceptors (quinones and ferricyanide), both aerobically and anaerobically. PSII crystals exhibit the highest quantum yield of O_2 production yet observed of any native or isolated PSII (61.6%, theoretically 59 000 μmol O_2/mg Chl/h). WOC cycling can be sustained for thousands of turnovers only using an electron acceptor (quinones, ferricyanide, etc.). Simulations of the catalytic cycle identify four distinct photochemical inefficiencies in both PSII crystals and dissolved PSII cores that are nearly the same magnitude. The exogenous acceptors equilibrate with the native plastoquinone acceptor at the Q_B (or Q_C) site(s), for which two distinct redox couples are observable that regulate flux through PSII. Flux through the catalytic cycle of water oxidation is shown to be kinetically restricted by the Q_AQ_B two-electron gate. The lifetimes of the S2 and S3 states are greatly extended (especially S2) by electron acceptors and depend on their redox reversibility. PSII performance can be pushed *in vitro* far beyond what it is capable of *in vivo*. With careful use of precautions and monitoring of populations, PSII microcrystals enable the exploration of WOC intermediates and the mechanism of catalysis.

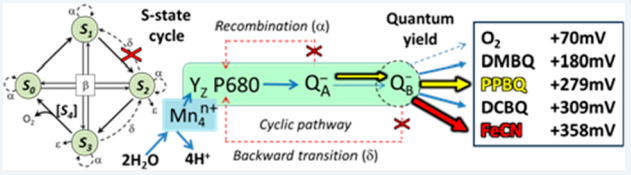

KEYWORDS: *photosystem II, (micro)crystals, oxygen-evolving complex, S states, quantum yield, electron acceptors*

INTRODUCTION

Photocatalysis of water splitting into protons, electrons, and oxygen is considered an indispensable requirement for utilizing solar energy for both energy storage and a future hydrogen economy. Nature has evolved a singular enzyme for performing this reaction across all organisms capable of oxygenic photosynthesis: photosystem II (PSII). The atomic structure of cyanobacterial PSII has been elucidated in atomic detail by crystallography, but state-of-the-art functional characterization of the four-step photocatalytic cycle from PSII crystals has lagged behind. The first crystal structure of PSII was solved at a resolution of 3.8 Å by Zouni et al. in 2001,[1] after which crystal structures at increasing resolution were published, progressing to 3.7 Å,[2] 3.4 Å,[3] 2.9 Å,[4] and by 2011 to 1.9 Å,[5] high enough that the near-atomic structure of the enzyme can be observed. Discrepancies were observed between crystal structures determined and spectroscopic results which indicated that X-ray induced damage may alter the structure of the water oxidizing complex (WOC).[6−8] It should be noted that the improvement in resolution was achieved by partial dehydration of the crystals leading to very tight packing that may limit conformational changes in PSII including quinone exchange. The recent advent of the X-ray free electron laser, which provides ultrabright ultrashort X-ray pulses of 10−50 fs pulse duration, capable of obtaining structural data prior to structural damage,[9,10] allows for diffraction data to be serially collected at room temperature leading also to the first time-resolved X-ray crystallographic structures.[11−15] However, the interpreted results differ strongly, raising the question of whether PSII functionality, including the function of the WOC and quinone exchange, is maintained in the crystals. While crystals contain the most homogeneous form of PSII, the function of PSII may be altered when the molecules are extremely tightly packed, as is the case for several recent high resolution studies.[12,14,15] Loose packing of PSII in crystals limits resolution of Bragg diffraction, but allows for higher resolution structures to be determined with evaluation of continuous diffraction. The latter represents a single particle diffraction pattern of the four

Received: November 9, 2018
Revised: December 25, 2018
Published: January 4, 2019

DOI: 10.1021/acscatal.8b04513
ACS Catal. 2019, 9, 1396−1407

PSII molecules in the unit cell and allows for direct phasing of the data.[9,16] High-throughput methods for production of large numbers of extremely high purity microcrystals have been developed (Scheme 1), allowing the further expansion of high-

Scheme 1. Preparation and Investigation of High-Purity PSII Microcrystals

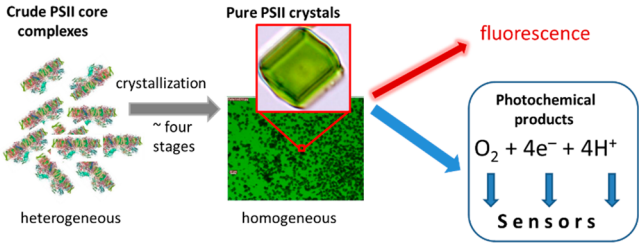

resolution SFX data to be collected on PSII crystals that are not dehydrated. These microcrystals, in addition to being extremely high purity, retain almost 100% of activity for months in storage at 4 °C or days on the benchtop.[9,11]

There are multiple expected benefits to use of crystals for study and understanding of the mechanism of water oxidation; however, one must cleanly control formation of individual intermediate states in the catalytic cycle (S states). The challenges are 3-fold: solving the ambiguity over both the resting populations of the four individual S states in the dark and their respective spin isomers (two, three, or more per S state), the difficulty of cleanly advancing through the cycle using flashes owing to intrinsic limitations in PSII photochemistry (misses, etc.), and to insufficient light saturation at high optical density.[12,15,17,18] However, the success of a photooxidation flash applied to PSII microcrystals has yet to be accurately determined for a series of multiple flashes. Thus, several contradictory models of the WOC mechanism and the structures of the intermediates in higher S states have been published and the discrepancies are still unsolved.[12,15,19−22] Experimental evidence of dark S state populations, isomers, and fidelity of flash-induced S state advances in PSII crystals are necessary to clarify what a given crystal structure shows. This information is presently lacking. Only recently have simple attempts been made to address the matter via quantitative measurements of PSII operation,[12,15,23] and this approach has been limited by the same fundamental assumptions which lead to conflicting evidence and interpretations. The results reported do not sufficiently take into account the possibility of various inefficient processes within PSII and assume ideal operation when there is no evidence to support this in PSII microcrystals. We undertook this study to provide a quantitative description of the PSII photocycle in microcrystals in order to inform the user community conducting crystallographic and spectroscopic studies.

In this research, we examine PSII microcrystals to determine their S state populations, lifetimes, and quantum yields as a function of flashes and light intensity, using a range of electron acceptors. In nature, PSII is embedded within the native membrane and equilibrates with excess plastoquinone/plastoquinol (PQ/PQol) from the pool within the thylakoid membrane. In crystals, maintaining oxygen evolution over multiple cycles of the WOC reaction requires supplemental electron acceptors, as in their absence PSII may even form reactive oxygen species where dissolved O_2 serves as a (poor) electron acceptor. The choice of terminal electron acceptor can substantially alter the overall photochemical activity of PSII due to individual binding affinities and regulation by the endogenous Q_AQ_B plastoquinone electron carriers (Q_A and Q_B − primary and secondary quinone electron acceptor).

MATERIALS AND METHODS

Isolation and Crystallization of PSII. PSII dimers were isolated from *Thermosynechococcus elongatus* as described previously.[11,24,25] Briefly, the intact PSII dimer is solubilized, starting from purified core complexes, into detergent micelles using ultrapure, stereochemically pure beta-dodecylmaltoside (β-DDM) (Glycon Biochemicals) as detergent. As this complex contains 70 chlorophyll/PSII dimer, the protein concentration is determined on the basis of the chlorophyll (chl) concentration. In order to solubilize this complex in its most active form a fixed ratio of detergent to chl of 0.7% β-DDM to 0.5 mM chl is necessary. The PSII-dimer-detergent micelle is purified by tentacle ion exchange chromatography (Toyopearl) and further purified by four rounds of recrystallization. PSII is crystallized in batch at 0.5 mM chlorophyll concentration using PEG2000 as a precipitant and repeated four times after resolubilizing by dilution of chl. In each recrystallization step, the PEG concentration is decreased, performing the initial precipitation at 7.5% PEG, the second step at 6.5% PEG, the third step at 5.5% PEG, and the last step at 4−5% PEG. The crystallization steps were performed in buffer consisting of 100 mM PIPES at pH 7.0, 5 mM $CaCl_2$, 10 mM tocopherol, and 0.02% β-DDM. Crystals were uniformly 10−12 μm in diameter as determined by optical microscopy (inset to Scheme 1). Measurements of crystals were done in stabilizing buffer: 100 mM PIPES at pH 7.0, 5 mM CaCl2, 10 mM tocopherol, 20% PEG 2000, and 0.02% β-DDM.

Light Excitation. To attain sufficient intensity across the visible spectral region, we used a high pressure Xe flash lamp (model ISSh-400, Soviet Air Force). The flash duration at half-maximum (fwhm) is about 1 μs and the delivered optical energy was adjusted to achieve maximum O_2 yield, as shown in Figure 1. Based on the measured flash profile, 99% of the energy is delivered in pulse of under 15 μs duration.

Flash Oximetry. All O_2 measurements were carried out using a Pt−Ir working electrode covered by ultrathin membrane (rate electrode).[26] The small sample chamber volume (8 μL) and 4 mm diameter results in rapid consumption of O_2 from the sample when it is sealed with a glass cover for anaerobic conditions. A Teflon ring spacer was added to produce aerated conditions, as described in the figure legend. The membrane prevents diffusion of added electron acceptors to the electrode surface.[27] All measurements were conducted using a constant DC voltage bias without an AC filter. All O_2 signals are directly proportional to the current needed to reduce O_2 to water. The O_2 yield was obtained by integration of the current pulse and using Faraday's law ($4e^-/O_2$). Crystals were diluted to a working concentration of approximately 4800 crystals per μL of sample and uniformly spread to avoid shading effects on the electrode. At working concentration, the crystals have sufficient area to cover only 30% of the electrode surface, thus minimizing the likelihood of crystals shading other crystals during measurements. This conclusion was confirmed as the O_2 signals were a linear function of the crystal content. To prevent precipitation of microcrystals in oxygen microcell 10% Biogel P-10 was used, which was acquired from BioRad.

DOI: 10.1021/acscatal.8b04513
ACS Catal. 2019, 9, 1396−1407

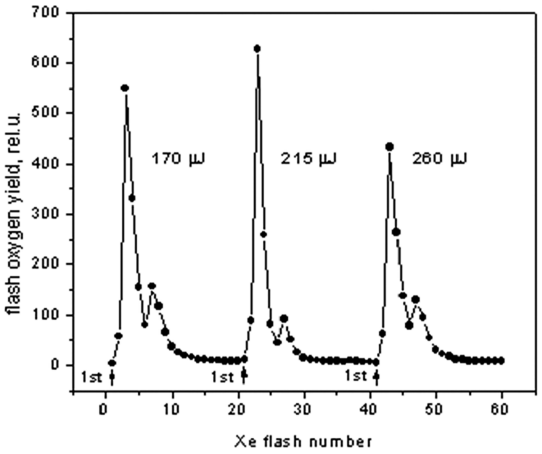

Figure 1. Flash O_2 yield dependence from PSII microcrystals on xenon flash lamp energy (given in μJ) using 1-μs flashes. Samples were dark-adapted for 10 min prior to each flash train (not shown in figure) and fresh samples were used for each light intensity. These measurements were conducted in aerobic conditions in the absence of any electron acceptor at room temperature. Twenty flashes per train were applied at 0.5 Hz. Data shown is representative of three replicate experiments.

The flash-induced O_2 signal from microcrystals detected by the rate electrode reflects current generated by O_2 reduction, and requires 2 s to return to the baseline (95% recovery), which limits the flash rate to slower than 0.5 Hz. However, such slow integration cannot avoid loss of some S state populations because of deactivation during the dark period between flashes. For this reason the oxygen yield was obtained using the difference between the preflash minimum and the maximum peak which occurs within 0.8 s for each O_2 kinetic curve. This method allows the O_2 current to replace the O_2 charge under the integrated curve for relative measurements and reduces losses from S state decay.

Evaluation of O_2 Evolution Data. Model-independent analysis of oxygen yield was performed via Fourier transformation to determine the flash frequency distribution that produces O_2.[28] Model-dependent analysis of the WOC cycle was done by fitting the O_2 flash yields to a four-parameter asymmetric Markov model denoted VZAD (Vinyard, Zachary, Ananyev, and Dismukes model), as described in prior work.[27,29] VZAD fitting accuracy was determined by nonlinear least-squares RMS deviation of the fit. Quantum yields of oxygen evolution were determined by dividing the oxygen yield per D1-PSII by the theoretical maximum oxygen evolution from a saturating flash in a fully scrambled population, 250 mmol O_2 per mol D1.

Electron Acceptors. Synthetic quinones 2,6-dichlorobenzoquinone (DCBQ), 2,5-dimethyl-*p*-benzoquinone (DMBQ), and phenyl-*p*-benzoquinone (PPBQ) were obtained from Aldrich Chemical Co. (98% purity). These were purified by double recrystallization in ethanol and subsequently dissolved in dimethyl sulfoxide (DMSO) at 10 mM concentration, and they were further diluted into samples for experiments. $K_3Fe(CN)_6$ (potassium ferricyanide, abbreviated FeCN below) was obtained from Sigma-Aldrich (99% purity).

RESULTS

Optimizing Light Intensity. Cyanobacterial PSII contains a core antenna system consisting of 31-antenna Chl per PSII monomer plus 4-reaction center Chl which are part of the electron transfer chain. In addition to receiving excitation energy directly from the core antenna, phycobilisomes are associated with PSII on the stromal side and serve as a peripheral antenna system that absorbs light in the "green gap". As PSII microcrystals do not contain phycobilisomes, they are solely reliant on chlorophylls (35 Chl/PSII) for light capture and charge separation.[11] This decreases the cross section for light capture by at least an order of magnitude as compared to living cells. Accordingly, it is necessary to supply a far greater light intensity to achieve saturation of photochemical steps in core complexes.[15,18,27,30,31] The saturating light intensity in a microcrystal system must therefore be empirically determined as demonstrated in Figure 1.

From left to right in Figure 1, flash intensities of 170, 215, and 260 μJ (optical energy; 13.5, 17.1, and 20.7 μJ/mm^2 delivered to the thin layer of crystals) from a xenon flash lamp were tested to determine saturation of O_2 yield. Peak O_2 yield was observed at 215 μJ, while less O_2 was produced at both 170 μJ and even less at 260 μJ. As no external quinones were added, only dissolved O_2 from air or residual plastoquinone could serve as electron acceptor. In principle each PSII should only be able to produce a maximum of one cycle of oxygen, as the oxidized internal Q_A and Q_B acceptors can be reduced by a total of three electrons without reoxidation. However, as seen, some oxygen is still evolved in the second cycle, even under optimized light intensity, indicating another electron acceptor is present. At subsaturating light intensities (170 μJ), a larger fraction of PSIIs do not produce O_2 on the first cycle and have an increased second cycle yield because of greater photochemical misses. At 260 μJ the total yield is decreased, indicating that too much light caused photoinhibition. The light intensity dependence of O_2 evolution from dissolved PSII cores has very similar dependence, as described later (Figures S1 and 8B).

Effect of Oxygen. The next set of experiments studied how the presence of O_2 in air influenced the flash-induced O_2 signal in the absence of synthetic electron acceptors. It was previously shown that dissolved O_2 can serve as an electron acceptor from Q_A^- and/or Q_B^{2-} in spinach PSII membrane fragments, where up to 15% of generated electrons may be directed to oxygen.[32] To test the turnover efficiency of PSII microcrystals, we performed two experiments under aerobic and near-anaerobic conditions (Figure 2)

A 20% decrease in the integrated flash O_2 yield from the first flash train (with most oxygen coming from the first four flashes) is observed under near-anaerobic vs aerobic conditions (Figure 2A). The oxygen yield continues to decline with each train under near-anaerobic samples, dropping to under 20% of the initial oxygen evolving activity by the end of measurements. The remaining oxygen evolving activity is likely due to use of some of the O_2 produced by the WOC as an electron acceptor. In air, a decline to 83% of the initial activity is observed on the second train and is followed by a much slower loss of activity, only 5% more over the next 10 flash trains. This shows that crystallized PSII has the capacity to accept three endogenous electrons under anaerobic conditions, and that dissolved oxygen can serve as a terminal electron acceptor on a slow time scale, faster than the 10 min dark period between trains, but far slower than the 2 s time between flashes.

Quantum Yield and Efficiency of PSII Microcrystals. The decrease in oxygen-evolving activity can be completely ameliorated by adding a fast-acting electron acceptor such as

DOI: 10.1021/acscatal.8b04513
ACS Catal. 2019, 9, 1396−1407

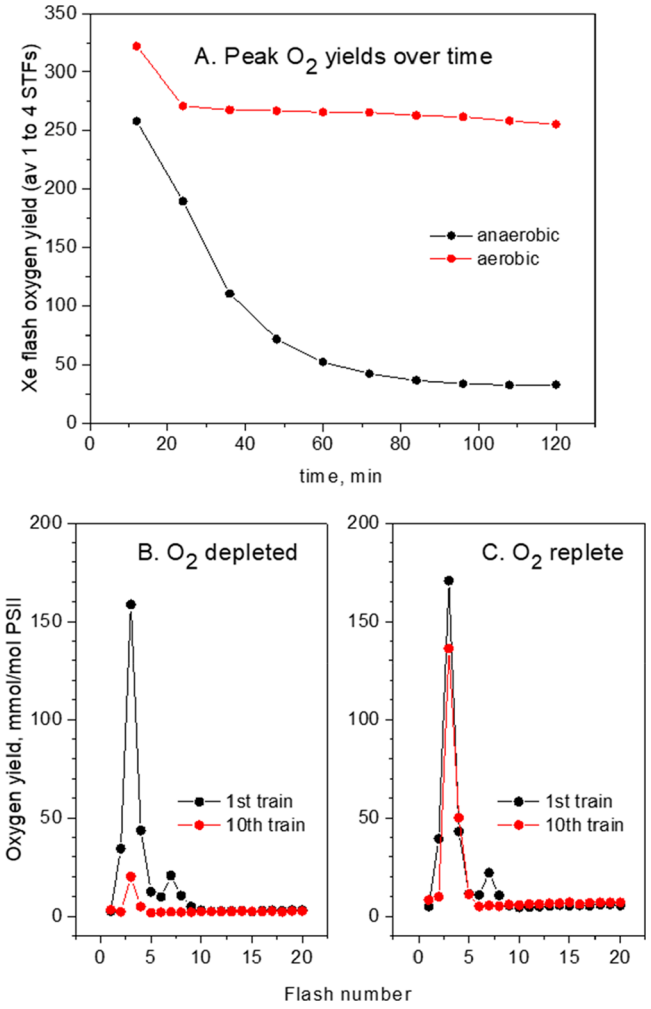

Figure 2. (A) Average of the flash oxygen yield on the first four (single turnover) flashes per PSII from a microcrystal sample under aerobic and anaerobic conditions with no exogenous electron acceptors. To bring most of the PSII complexes in the crystals to the S1 state, the crystals were subjected to one preflash then 10 min dark preincubation time following the preflash, before exposure to a train of 20 1-μs Xe flashes at 0.5 Hz. This sequence was repeated 10 times with 10 min dark preincubation before each sequence. (B) and (C) show the raw data for the first and tenth train of 20 flashes for near-anaerobic (residual oxygen content about 0.5 mmol O_2/mol PSII, or too little signal to be clearly distinguished from electrical noise) and aerobic samples. Near-anaerobic conditions were achieved by sealing the chamber during preincubation to allow the electrode to consume residual oxygen.

PPBQ and FeCN. The use of acceptors to allow for electron transfer to continue over several cycles to maintain or increase PSII activity and oxygen evolution is universally recognized and widely reported.[27,30,33−37] All acceptors used herein are well established to accept electrons from PSII.[37−39] The aim of our studies here is to establish which one produces the highest O_2 flash yields and sustains the oscillations over the largest number of flashes for use in turnover and S state lifetime studies. We monitored the steady-state oxygen yield (yield-SS), the average yield from the first four flashes (yield-4F), and the number of sustained oscillations using PPBQ, DMBQ and FeCN (Figure 3). Aerobic conditions were used, as oxygen is a necessary acceptor over long dark periods but has negligible effect within individual trains.

The quantum efficiency of oxygen evolution in vivo[27] and in vitro[40,41] is often substantially lower than the theoretical maximum of one molecule of oxygen per D1 on every fourth saturating flash, ranging from under 2% to about 33% in prior reports.[27,30,33,41,42] The source of this low quantum efficiency is a combination of native inefficiency processes (misses, backward transitions, and photoinactivation of active PSII centers, WOC reduction by photoaccumulated quinols etc., and inactive PSIIs). The existence of at least some nonfunctional PSII in all but the highest-purity core complexes is known.[43] In PSII microcrystals, the observed range of quantum yields (and quantum efficiencies) depends strongly on the electron acceptor system (Figure 4).

With optimization of electron acceptors, PSII microcrystals can greatly surpass the previous record oxygen quantum yields from noncrystalline PSIIs. Furthermore, the characteristic loss of activity during a flash train in the absence of added acceptor can be prevented; at optimal concentration of PPBQ the initial activity on the first cycle is 60% higher (yield-4F = 103.3, Figure 4) than with no acceptor (only air). Only a minimal loss of O_2 evolving activity was observed over a train of 30 flashes (yield-SS = 103.3, Figure 4). Other quinones give lower yields (DCBQ and DMBQ, Figure 4 and Table 1). As accumulation of the reduced quinol (QH_2) continues during illumination, the O_2 yield drops below that observed with FeCN alone, as shown in Figure 5B. This indicates that in addition to lower yield due to consumption of the quinone, the accumulation of the quinol leads to inhibition of oxygen evolving activity, driving it below the level of activity seen with FeCN. This reduction of activity is reversible upon removing the supernatant and restoring the original electron acceptors, indicating that PSII is not photoinhibited (see Figure S1). This is described further in the next section. In support of this interpretation, prior studies have indicated that accumulation of reduced PQH_2 in native membranes, caused by reduction of the PQ pool, leads to a proportional increase of backward transitions at the WOC.[27,30]

Ferricyanide (FeCN) is a water-soluble one-electron reversible oxidant with midpoint potential +358 mV (varies with environment[36]), sufficient to oxidize both the semiquinone anion radical and the quinol forms of all three acceptors studied herein. However, reaction with the quinol form is slow as this requires a proton acceptor better than water. By contrast, reaction with the semiquinone anion is fast as it requires no acceptor.[34,36] It is also a well-known, albeit comparatively inefficient, electron acceptor for PSII.[44] Use of both a quinone and FeCN together as electron acceptors produces a larger increase in O_2 yield than either one alone for all quinones studied. PPBQ+FeCN yields the largest increase, by more than 2-fold. Combining these electron acceptors gives the greatest number and amplitude of visible oscillation periods (over 25 visible cycles in Figure 3D) and yields a record quantum efficiency for O_2 production of 61.6%.

FeCN and PPBQ do not act solely at the same (Q_B) site within PSII[36] and as expected support very different O_2 flash yields as seen in Figure 5A,B. In the presence of PPBQ alone, 3-fold more oxygen is initially evolved than in the presence of FeCN alone, 110 mmol/mol PSII vs 32 mmol/mol PSII, using the optimal concentration of each. PPBQ is the preferred electron acceptor, as further indicated by Figure 5C, showing the two phases of acceptor control (5A and B) effectively superimposed on one another with the PPBQ phase coming first. By integration of these traces, it is possible to determine

DOI: 10.1021/acscatal.8b04513
ACS Catal. 2019, 9, 1396−1407

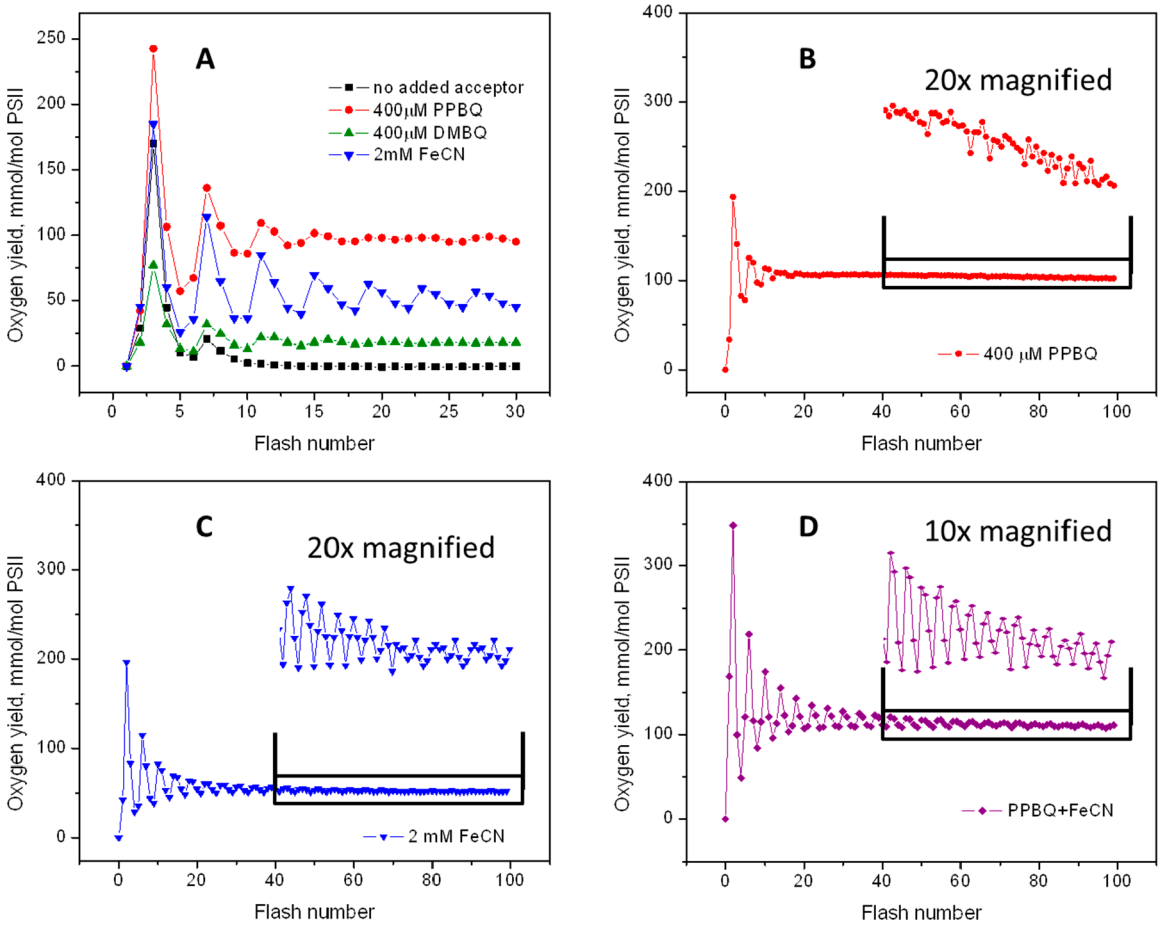

Figure 3. (A) Sustained oscillations of oxygen flash yield from dark-adapted suspensions of PSII microcrystals in the absence of electron acceptors (black) or in the presence of 400 μM quinone acceptor (PPBQ, red, or DMBQ, green) or 2 mM ferricyanide were subjected to one train of 20 saturating Xe flashes at 0.5 Hz under air headspace. Comparison of (B) PPBQ and (C) FeCN as sole acceptors to the best acceptor pair (D) 400 μM PPBQ plus 2 mM FeCN. Insets to (B), (C), and (D) show expansion of oscillations from flashes 40−100. Optimal electron acceptor concentrations were determined via titration for oxygen yield (Figure S2). Representative data from a set of three replicates are given.

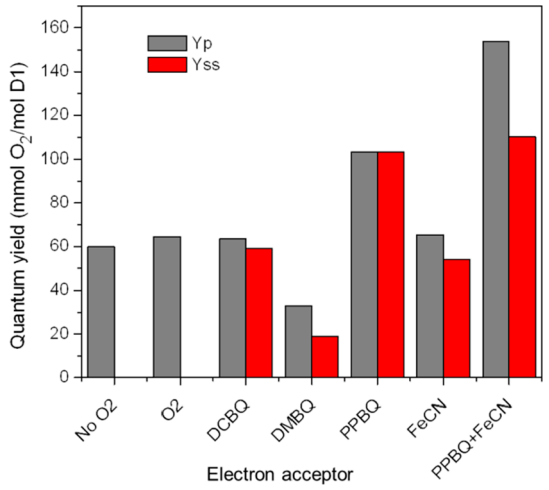

Figure 4. Effect of electron acceptors and dissolved oxygen on the quantum yield of flash-induced oxygen (QY = oxygen molecules produced per 1000 PSIIs per flash). Gray: Average yield from the first four flashes (yield-4F). Red: Average yield at steady-state (yield-SS). QY = 250 is equivalent to one molecule of oxygen evolved per WOC every four flashes, the theoretical maximum for a four-photon WOC cycle. Measurement conditions were as described in Figures 2 and 3; 400 μM DCBQ was used where denoted.

the relative electron capacity of the acceptor pool from the number of molecules of oxygen generated over time. The 2 mM FeCN supplied approximately 5000 electron-holes per PSII, while the 400 μM PPBQ removed a further 2000 electron-holes (being able to accept two electrons rather than one). Of these acceptor pools, 370 electrons were accepted by the PPBQ alone and 550 by the FeCN, while the acceptors used together were able to take up 870 electrons. Areas integrated to obtain yields are shown in yellow in Figure 5. The end point in these titrations, where zero O_2 activity is reached, occurs more quickly using only PPBQ and no FeCN after 12 flash trains (1440 flashes). This compares to 37 flash trains (4440 flashes) with both PPBQ and FeCN, and 50 flash trains (6000 flashes) with FeCN alone. The integrated yield of O_2 produced by the two individual acceptors is only slightly less than the yield produced when the two acceptors are combined together.

Taken together, these data on the peak positions, integrated electron capacities and chemical preference for distinct terminal electron acceptors indicate the presence of two *internal* electron acceptors in PSII that control the yield of O_2. These distinct internal electron acceptors possess increasingly more positive reduction potentials, presumably $(Q/Q^-)_A$ and $(Q/Q^-)_B$, although we do not exclude the putative Q_C site (proposed quinone site within PSII) as a possibility.[4]

DOI: 10.1021/acscatal.8b04513
ACS Catal. 2019, 9, 1396−1407

Table 1. PSII S State Populations and Inefficiency Parameters Obtained from Fitting the Data in Figure 7B,C to the WOC Cycle Model[ψ]

VZAD Parameter	Cells *T. elongatus*[b]	PSII microcrystals (vs. dissolved) *T. elongatus*[a]	
		Flashes 1-30	Flashes 31-100
α, miss	0.100	0.058(0.077)	0.014(0.030)
β, double hit	0.051	0.014(0.016)	0.000(0.002)
δ, backward transition	0.000	0.069(0.080)	0.000(0.011)
ε, inactivation	0.010	0.037(0.075)	0.004(0.006)
S0 dark population	0.389	0.105(0.062)	0.243(0.264)
S1 dark population	0.444	0.641(0.712)	0.259(0.260)
S2 dark population	0.166	0.254(0.226)	0.262(0.239)
S3 dark population	0.009	0.000(0.000)	0.236(0.237)
Experimental FT Period	4.160	4.139(4.172)	4.037(4.110)
Theory FT Period	4.206	4.341(4.450)	4.057(4.156)
Electron acceptor for PSII microcrystals: [a]400 μM PPBQ + 2 mM FeCN [b]250 μM DMBQ Right: The WOC cycle and VZAD parameters[29]			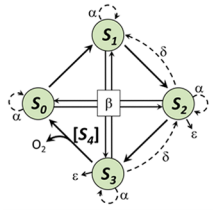

[ψ]400 μM PPBQ, 2 mM ferricyanide, 10 min dark pre-adaptation time. Data from living culture obtained from *T. elongatus* cells supplemented with 250 μM DMBQ (optimal acceptor for in vivo conditions) at room temperature.[33]

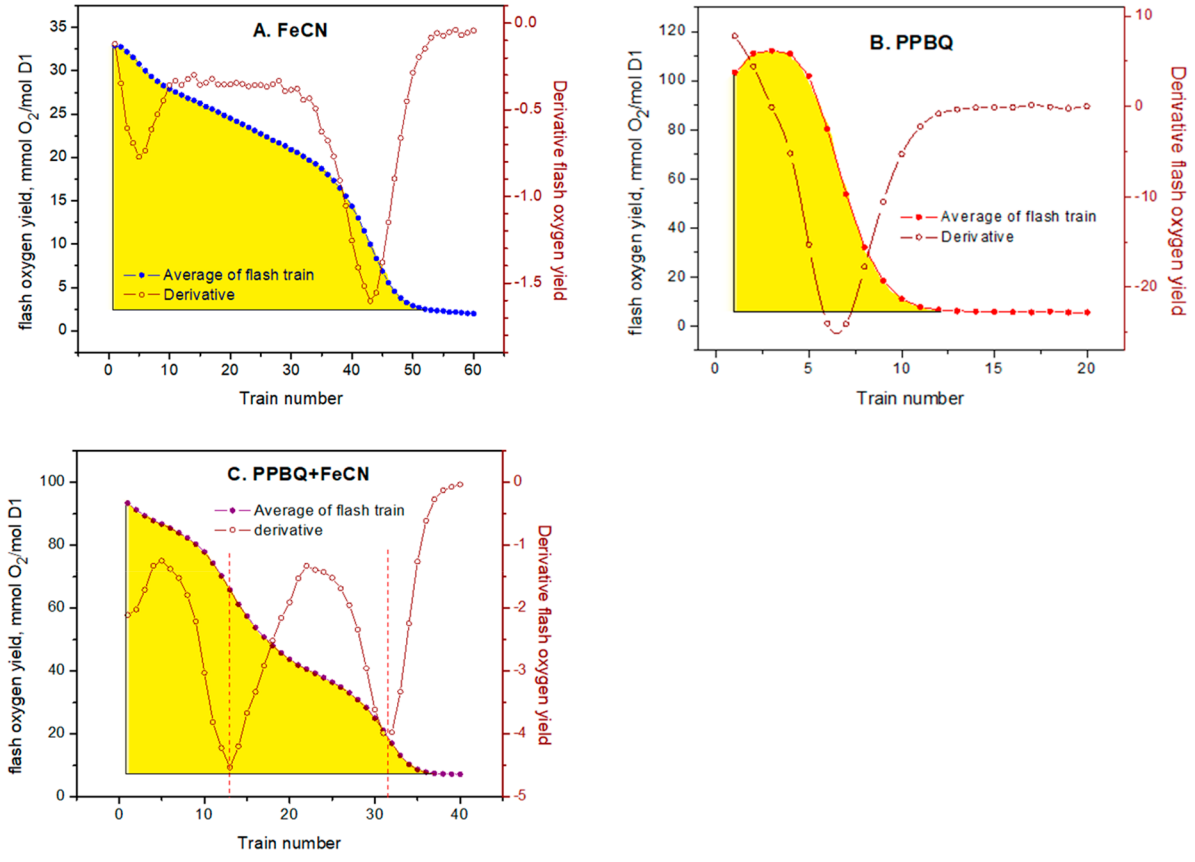

Figure 5. PSII-dependent photoreduction of terminal electron acceptors by light. Oxygen evolution of dark-adapted PSII microcrystals in suspension in the presence of (A) 2 mM FeCN, (B) 400 μM PPBQ, and (C) both PPBQ and FeCN. The crystals were subjected to a series of flash trains of 120 saturating xenon flashes at 0.5 Hz flash rate under oxygenated headspace. The average oxygen yield from 120 flashes (each flash train) is plotted. Representative data from a set of 3 replicates are given. The derivative of the oxygen yield during illumination is overlaid on the data. Areas integrated to obtain total oxygen yield are shown in yellow.

DOI: 10.1021/acscatal.8b04513
ACS Catal. 2019, 9, 1396−1407

Table 2. Decay Kinetics of the S2 and S3 States from *Thermosynechococcus elongatus* Living Cells (with and without Addition of 250 μM DMBQ),[33] Thylakoids Supplemented with 500 mM DCBQ,[62] PSII Core Complexes Supplemented with 500 mM DCBQ,[61] and Microcrystals Supplemented with 2 mM FeCN (Figure 6), As Measured at Room Temperature[a]

sample and S state	t1, s	A1	t2, s	A2	y0
living cells, S2	8.6	0.14	350	0.19	0
living cells + 250 μM DMBQ, S2	19.7	0.13	450	0.23	0
thylakoids + 500 mM DCBQ, S2	n/a	n/a	450	0.63	0
PSII cores + 500 mM DCBQ, S2	55.6	0.49	2200	0.08	0.09
microcrystals + 2 mM FeCN, S2	4.0	0.13	1500	0.24	0.09
living cells, S3	9.8	0.15	240	0.18	0
living cells + 250 μM DMBQ, S3	5.7	0.14	550	0.22	0
thylakoids + 500 mM DCBQ, S3	7.8	0.48	290	0.15	0
PSII cores + 500 mM DCBQ, S3	13.4	0.08	83.0	0.47	0.09
microcrystals + 2 mM FeCN, S3	2.3	0.24	400	0.33	0.02

[a]A1 (fraction of centers involved in fast decay), A2 (fraction of centers involved in slow decay), and y0 (fraction of centers modeled to not decay during measurement) values are given in fraction of the total population of PSIIs and are specific to starting conditions.

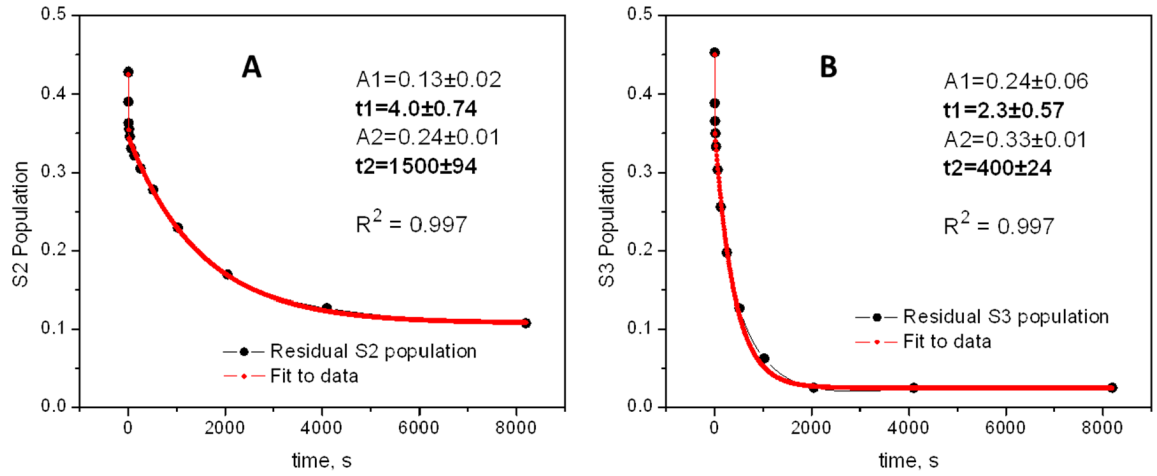

Figure 6. Lifetimes of the flash-induced (A) S2 and (B) S3 populations of the WOC in the dark in PSII microcrystals supplemented with 2 mM FeCN, as measured oximetrically. Individual populations of S2 and S3 states were calculated using the VZAD model (see Table 1)[29] and the populations given on the *Y*-axes reflect the fraction of active centers in each state. Inset gives the fits to a biphasic decay model with 1/e lifetimes t1 and t2 (seconds) and relative populations A1 and A2.

S State Populations and Lifetimes. Dark stable S state populations and decay lifetimes vary substantially with the degree of PSII fractionation and in microcrystals (Table 2). This distinction has not been fully appreciated and can lead to conflicting accounts. We investigated the lifetimes of the S2 and S3 states as reached by single (S2) or double (S3) flash excitation of dark-adapted PSII microcrystals using FeCN as an electron acceptor (Figure 6). An electron acceptor is necessary to produce the multiple periods of oscillations in O_2 yield needed to accurately model the WOC cycling, from which the dark populations are determined. We used the VZAD model to fit the oscillations (shown in Figure 3C), yielding the four inefficiency parameters of the WOC cycle and the dark populations (Table 1).[29,45,46] The results show that in the presence of FeCN, the lifetime of S2 becomes extraordinarily long, with biphasic exponential fits (inset) revealing both short (4 s, 13% of centers) and long (1500 s, 24% of centers) 1/e lifetimes that decay to a nonzero baseline representing an even longer (third) S2 component (Figure 6A), which can be seen from the lack of a distinct 1/e component to decay on a time scale of hours to days or longer. Under these conditions, even after 2 hours in the dark, 10% of the total population remains in the S2 state. The S3 population decays via biphasic exponential kinetics with both short (2.3 s, 24% of centers) and long (400 s, 33% of centers) lifetimes that decay to a near-zero baseline (<3% amplitude). These are essentially normal lifetimes, comparable to the decay time observed in living cells.[33]

Modeling the WOC Cycle in PSII Microcrystals. Fitting of the oscillations in O_2 yield to the VZAD model reveals the underlying inefficiencies of the WOC cycle that best fit the data. In most PSII-containing preparations other than crystals, the initial oscillations in oxygen yield seen in dark-adapted samples damp quickly in a few cycles to a steady state (nonoscillating) value. In contrast, the 10 min dark adapted crystals show period-4 oscillations for more than 100 flashes at flash rate of 0.5 Hz. We used the VZAD model of the WOC cycle to obtain the best fit of the oscillations in O_2 yield by minimizing the residuals.[29] This asymmetric Markov model assumes a single four-step catalytic cycle with four inefficiency parameters, depicted in Table 1. The model does not correct for S state decay between flashes. As seen in Figure 7A, the entire set of 100 flashes does not fit the full range of oscillations simultaneously very well (see residuals). To achieve the best fit to the initial decay, the model predicts stronger initial damping, which results in unobservable oscillations later and a larger photoinactivation rate (negative slope) than actually observed. However, splitting the data into

DOI: 10.1021/acscatal.8b04513
ACS Catal. 2019, 9, 1396−1407

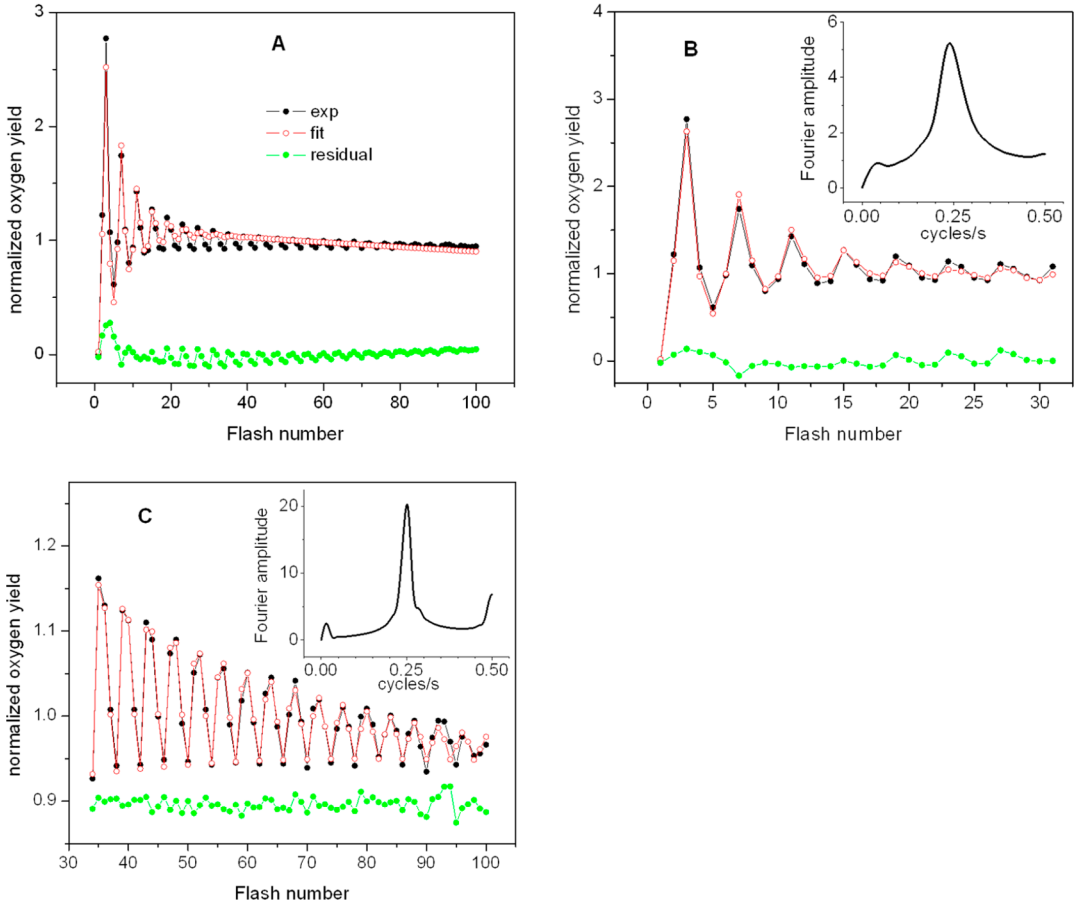

Figure 7. Dark-adapted PSII microcrystals in aerobic solution supplemented with 400 μM PPBQ and 2 mM ferricyanide were subjected to 100 saturating xenon flashes at 0.5 Hz flash rate and repeated three times after dark adaption for 10 min prior to each flash train. Data shown are the average of three biological replicates. Raw data (seen in Figure 3D) were normalized to yield-SS = 1 (yield-ss: yield of oxygen from a flash train at steady-state). (A) VZAD fit to all 100 flashes; (B) VZAD fit to flashes 1−30; (C) VZAD fit to flashes 31−100. Inset shows the Fourier transform of each experimental data set. Residuals given for each fit; residual in (C) was offset +0.9 for ease of display.

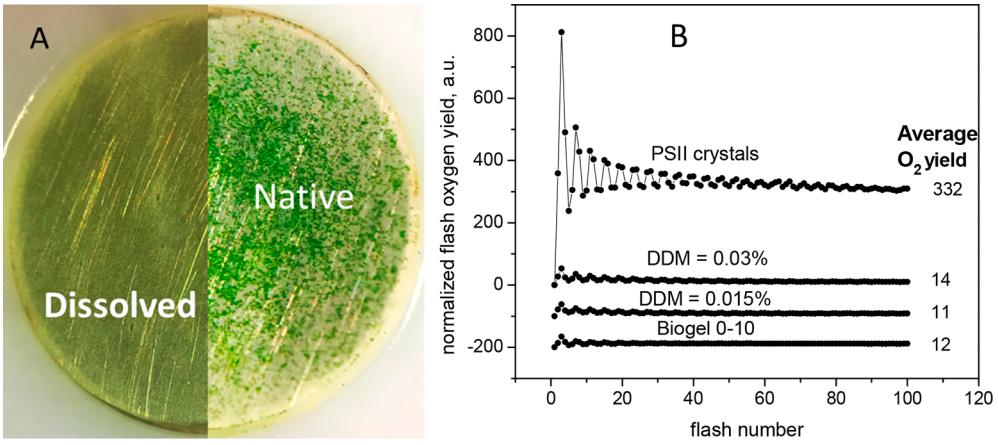

Figure 8. (A) Optical microscope image showing on left, dissolved PSII microcrystals in solubilization buffer (core complexes in detergent micelles), and on right, PSII microcrystals, on the surface of the membrane-covered Pt−Ir electrode. (B) Raw flash oxygen yield measurements of "native" precipitated and uniformly suspended PSII microcrystals and dissolved PSII core complexes, both supplemented with 2 mM FeCN. The data for dissolved PSII cores in 0.015% DDM and intact PSII microcrystals suspended in Biogel are offset for clarity (average O_2 yields are listed). Figure S5 shows a magnification of the data corresponding to the PSII core complexes in 0.03% DDM solution. Flash energy = 215 μJ.

two segments over shorter intervals of the initial 30 and 31−100 flashes fits very well, as seen in Figure 7B,C. The resulting four inefficiency parameters and initial (dark) S state populations for both ranges are given in Table 1. During the initial 30 flashes, the WOC cycling exhibits strong damping with larger misses and backward transitions, whereas after the first 30 flashes there is a much smaller loss in oscillation amplitude and both parameters drop by 4-fold or more. Model-independent Fourier transformation of the experimental data, shown in the insets and Table 1, reveals that the width

DOI: 10.1021/acscatal.8b04513
ACS Catal. 2019, 9, 1396−1407

of the distribution around the period-4 oscillations dramatically narrows by 3-fold, while the Fourier transform peak shifts from 4.14 to 4.04, closer to the ideal (undamped) period-4. These changes suggest that the WOC cycle becomes significantly more efficient during flashing, as the PSII centers change from dark adapted to light adapted forms. Considering the biphasic lifetimes of S2 and S3 (Figure 6), the oscillations seen at greater flash number must come from PSII centers with the slower decaying populations. The S state populations predicted by VZAD confirm this expection, showing that all four S states become equally populated (Table 1).

The fitting parameters in Table 1 show that the misses are strongly decreased in the crystals as compared to living cells of *T. elongatus*. During flashes 31−100 there is a 4-fold decrease in misses to 1.4%, which is the smallest miss parameter ever observed in any PSII. Likewise, the other three inefficiency parameters decrease to near zero. The retention of weak period-4 oscillations indicates that the contributing PSII centers retain an elevated level of synchronized S states in the crystals and these represent the most efficient PSII centers ever observed. These extended oscillations only occur in crystals in the presence of exogenous electron acceptors (quinone), indicating the high homogeneity of PSII centers is needed to observe them. The long lifetimes of the S state populations and minimal losses continue until accumulation of the reduced quinols results in short circuiting by directly reducing the WOC. Comparing turnover of PSII in microcrystals vs living cells containing an exogenous quinone acceptor[33] (Table 1), the WOC S state populations in the dark shift from standard values to higher S states (S1 and S2 favored), and there is significantly more efficient operation (fewer misses and double-hits). Backward transitions and photoinactivations are small in both cases.

As shown in the photograph in Figure 8A, when these same microcrystals are dissolved in the solubilization buffer containing detergent micelles (i.e., above the CMC), a homogeneous solution is obtained. Crystal dissolution can be reversed by adding a 1:1 volume of polyethylene glycol buffer.[11] The resulting crystals have identical activity as the original crystals, with a negligible amount of PSII lost from the crystals. Figure 8B also shows that the yield of oxygen evolution from the same number of solubilized PSIIs (i.e., dissolved crystals) significantly decreases (Figure 8B), using identical flash intensity and electron acceptor concentrations. To determine the origin of this decrease, we considered the following four possibilities:

(1) Insufficient flash intensity: To test this, we generated a titration curve of oxygen yield as a function of the flash optical energy up to 260 μJ, as shown in Figure S1. Light saturation was achieved above 190 μJ; hence, we conducted our experiments at 215 μJ (peak).

(2) Insufficient electron acceptor capacity: To test this hypothesis we made sequential flash measurements and found that the steady state flash oxygen yield was the same for all sequential trains, as shown in Figure S3B. This indicates that the loss is not due to depletion of the electron acceptor.

(3) Reversible inactivation by the solubilization buffer: To test this we compared the O_2 yield of dissolved microcrystals in micelles at two different detergent concentrations, 0.03 and 0.015% DDM. There was almost no difference (<1%, Figure 8B), indicating no detergent inactivation. The decrease within each train could be due to the generation of reactive oxygen species due to the presence of detergent as described in.[47,48]

(4) Settling of the crystals on the bottom of the cell directly on top of the membrane where O_2 is detected: To test whether the location of the crystals in the cell influences the amount of O_2 reaching the electrode, we prevented settling of microcrystals by suspending them in the cell (10 μL volume, 0.3 mm vertical height, no mixing-unstirred) using a suspension of 10 μm-diameter polyacrylamide beads (Biogel P-10). The raw data for the uniformly suspended microcrystals and the solubilized PSII complexes are shown in Figure 8B. There we see that the microcrystals, when suspended in the cell produce flash oxygen yield nearly identical to that from the dissolved PSII core complexes (4% vs 5% of the settled crystals O_2). This shows that there is no significant difference in the optical cross sections of PSII core complexes whether suspended in micelles as individual complexes or condensed as microcrystals.

Figure S4 shows that the expanded oscillations produce a very high-quality signal which was Fourier transformed and fitted to the standard VZAD model. As before for the microcrystals, the entire range of flashes could not be fitted by one WOC cycle model and was split into two regions, the initial 30 and 31−100 flashes. The best fit parameters (lowest residuals) derived from the FT and VZAD fitting of the initial 30 flashes are given in Table S1. The WOC inefficiency parameters and dark S state populations are similar for PSII in crystals and micelles. The most notable difference is a 2-fold larger photoinactivation parameter for isolated PSIIs in micelles (ε = 0.075 vs 0.037), suggesting that removal of solvent and detergent in the packed crystals protects the system from photoinactivation.

DISCUSSION

Period-2 Modulation of O_2 Yield. The emergence of a strong period-2 feature following PSII-WOC cycling after 30 flashes is evident in PSII microcrystals. A weak period-2 feature has been observed previously in living cells that also occurs upon electron acceptor addition[27,30] and upon strontium substitution for calcium in the WOC.[33] Both of the latter changes are also accompanied by a longer S2 lifetime. A possible cause of this period-2 modulation of the O_2 yield in vivo was proposed over 20 years ago by Shinkarev[49] before any data to support it existed: different charge separation yields for the two redox transitions of the Q_B site (Q/Q^- and Q^-/QH_2). Shinkarev proposed that the limiting factor was the redox poise of the acceptor pool, with Q_B becoming trapped in the semiquinone form until reoxidation occurred and the overall redox poise changed.[49] Herein, the acceptor is provided in large surplus (7000 electron-holes per PSII). The sample environment is therefore not likely to become reduced as rapidly (not within 30 flashes). This allows many more synchronized oscillations to occur and a strong period-2 feature emerges. However, in vivo there is substantially less electron acceptor, with PQ pool sizes typically well under 50 PQ/PSII, and with PQ continuously replenished from PQH_2 reoxidation by Cytochrome b_6f.[27,33,34,50,51] Shinkarev's proposal may not be the only source of period-2 oscillations in isolated PSII microcrystals, and this interesting phenomenon should be addressed in the future.

DOI: 10.1021/acscatal.8b04513
ACS Catal. 2019, 9, 1396−1407

Quantum Yield. PSII O_2 quantum yields from cells in vivo and PSII core complexes in vitro, fall in the range 3.7%−35.2% and 0.7%−29.3%.[27,33,40,41,52−54] Without addition of electron acceptor, the PSII microcrystals are able to evolve O_2 for one turnover of the WOC cycle (three flashes) starting from mainly the dark S1 state. The integrated yield of O_2 from these three flashes corresponds to 42% of the O_2 produced on the first three flashes using the optimal electron acceptors. In untreated centers, two electrons can be accepted at the Q_B site, forming PQH_2, and a third electron reduces Q_A to its plastosemiquinone state. O_2 is evolved in a small fraction of centers on the fourth flash, but it is unclear whether this is due to an actual 4-flash advance from S0 or to misses.

S State Lifetimes and Populations. Historical experiments starting from illuminated whole cells and PSII enriched membranes have shown that dark adaptation results in depopulation of the unstable S3 and S2 states to form an S1 population yielding an approximate ratio of 0.75/0.25 = S1/S0.[55−57] When these samples are preflashed with one or two saturating light flashes, a decay of the S2 and S3 states to the dark S1 is observed in the time frame of seconds to several minutes (Table 2). The resulting unequal dark populations following decay are responsible for the period-4 oscillations of the flash-induced O_2 yield.[27,33,58−60] Analogous experiments done on detergent-solubilized thylakoids and isolated PSII core complexes produce the dark-adapted populations and S2 (S3) lifetimes given in Table 2,[61,62] although core decay was studied via EPR as opposed to the oximetric technique used for all other samples. Behavior of S state decay in PSII microcrystals is similar to that observed in core complexes; as compared to living cells, S3 decay favors the fast kinetic lifetime. The S2 state also sees a slight acceleration of the fast kinetic, but the dominant slow kinetic is further slowed by a factor of 3 and some centers (9% of total PSIIs) do not decay from S2 over 2 h.

A major challenge for researchers studying PSII microcrystals is how to form individual S states in controlled populations. The much longer dark lifetime of the S2 population in the presence of electron acceptor greatly slows repopulation of lower S states, which is the starting point for all standard flash studies of higher S states. However, elimination of the electron acceptor lowers the quantum yield, as flashes fail to advance centers without it. This paradox likely explains the substantial discrepancies in studies of PSII microcrystals by diffraction and spectroscopy.[12,15,17] These results clarify conflicting reports on the interpretation of the crystallography of flash-induced S2 and S3 states in PSII crystals that have no exogenous electron acceptors and unknown S state populations.

Without definitive evidence on S state populations, it is not possible to correctly use bond lengths determined from atomic coordinates by X-ray crystallography at high resolution to infer the formal oxidation states of the metal ions of the WOC, as has been attempted in a recent study of the metastable S states.[22] This approach to determine oxidation states is well ground in crystallography of simple transition metal ion complexes that lack stereochemical stress from ligands and which have one structural configuration defined by a single potential energy minima.[63] Neither of these conditions apply to the PSII WOC with its multiple spins states for each S state.

Regulation by Redox Poising. The choice of exogenous quinone as electron acceptor for PSII microcrystals has a major impact on the yield of O_2 (Figure 4), and the optimal quinone differs from PSII in whole cells.[27,33] Notably, DMBQ is a significantly poorer electron acceptor in PSII crystals than in cells, which can be attributed to its stronger binding of the reduced form, dimethylbenzoquinol, to the Q_B site. Similarly, only a small concentration of PPBQ is needed to reach near-maximum oxygen yield as compared to the requirement in living cells,[27,33] while accumulation of reduced $PPBQH_2$ causes a strong decrease in oxygen yield. This occurs because quinols like $PPBQH_2$ can donate electrons in two ways (refer to Scheme 2). First, directly to the WOC or tyrosine-Z via the

Scheme 2. Pathways of Electron and Proton Flow, Charge Recombination, and Backward Transitions in PSII, Showing the Difference between a Microcrystal System and Native Conditions

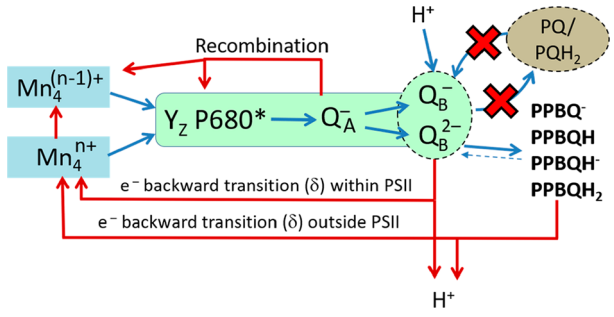

classic hydroquinol reduction and ADRY mechanisms on the donor side.[27,64−69] Alternatively, electron donation can occur from the PQH_2 pool (or from exogenous quinols) into the Q_B site forming the semiquinone radical anion. This is called a "backward transition" (δ, Scheme 2), and is the return pathway in cyclic electron flow around PSII.[27,29,30,33] Backward transitions increase in probability as the quinol accumulates during photolysis and can be slowed by adding an irreversible oxidant (FeCN) which rapidly oxidizes the semiquinone ($PPBQ^-$), thus allowing O_2 production to continue until the FeCN concentration drops below its binding threshold (i.e., is used up). This dependence of the light-induced flux through PSII on the ratio of reduced/oxidized terminal electron acceptor molecules allows regulation by either changing the size of the pool (i.e., total concentration), the ratio of plastoquinone/plastoquinol, or by adjusting the reduction potential by addition of exogenous acceptors. This phenomenon called "redox poising" or "redox buffering" occurs in vivo through the equilibration of binding between the pool of PQH_2/PQ molecules in the photosynthetic membrane and its functional binding site on PSII, the Q_B site for linear electron flow.[70−74] Another PQ site called Q_C may exist that is speculated to control PSII cyclic electron flow.[4,27]

PSII-WOC Core Complex Cycling in Micelles and Microcrystals vs Native Cells. After determining that PSII cores in micelles and microcrystals have nearly identical responses to light intensity, electron acceptor concentration/accessibility, are not inactivated by the detergent, and after correcting the O_2 electrode response due to the influence of microcrystal gravitational settling, we could directly compare the intrinsic WOC cycle inefficiency parameters obtained from the VZAD simulations and Fourier analysis. This reveals that PSII cores, whether in micelles or microcrystals, have very similar WOC cycling parameters, dark-adapted S state populations, and rapid transitions from dark- to light-adapted forms after 30 flashes (Table 1). The largest difference is the

DOI: 10.1021/acscatal.8b04513
ACS Catal. 2019, 9, 1396−1407

nearly 2-fold larger photoinactivation probability 7.5% (dissolved) vs 3.7% (crystals), further confirming the stabilizing influence of crystal packing. The dark-adapted form (flashes 1−30) is less efficient with >4 fold larger miss and backward transition probabilities. Both forms are appreciably more efficient than in living cells, which have a miss parameter of 10%.[27] The emergence of sustained period-2 oscillations following 30 flashes is a consequence of the longer lifetimes of S2 and S3 in microcrystals.

CONCLUSIONS

PSII microcrystals exhibit the highest O_2 quantum yield (61.6%) yet observed by far for any PSII preparation, which even exceeds the downregulated activity of PSII in vivo. This performance can be sustained over multiple flash cycles by utilizing an appropriate electron acceptor and removing or preventing accumulation of reduced electron acceptors (semiquinones and quinols). This activity is equivalent to 59 000 μmol O_2/mg Chl/h if operated continuously. However, such efficiency is not sustainable because of acceptor capacity limitation. Backward transitions account for an additional 7−8% of photonic energy capture in the form of cyclic electron flow around PSII which may be associated with proton pumping and ΔpH formation.[27]

The charge recombination lifetimes of the S2 and S3 states are much longer in microcrystals and controlled by the capacity and redox properties (reversible or irreversible) of the electron acceptors used. The latter operate through equilibration with the native Q_B (or Q_C) site, for which two distinct native redox couples are observable that control flux through PSII. The four-flash catalytic cycle of water oxidation (Kok cycle) that exists in dark adapted PSII centers is significantly more uniform and efficient in crystals than in vivo. This uniformity allows detection of a further modulation of the catalytic WOC cycle every two flashes, upon light adaptation and excess electron acceptors. Crystals of highly homogeneous PSII provide the best opportunity for exploring the limits of the operating capacity, regulation and mechanism of the enzyme.

ASSOCIATED CONTENT

Supporting Information

The Supporting Information is available free of charge on the ACS Publications website at DOI: 10.1021/acscatal.8b04513.

Line figures and explanation showing consumption of quinone electron acceptor by photoreduction from PSII and restoration when this additional acceptor is added. Line figures showing response of dissolved PSII microcrystals (core complexes) to a range of control conditions; one table comparing VZAD parameters to living culture (PDF)

AUTHOR INFORMATION

Corresponding Author

*E-mail: dismukes@chem.rutgers.edu.

ORCID

G. Charles Dismukes: 0000-0003-0155-0541

Notes

The authors declare no competing financial interest.

ACKNOWLEDGMENTS

This work was funded by the Department of Energy, Basic Energy Sciences, Grant DE-FG02-10ER16195 (to G.C.D. and G.A.), the NSF Science and Technology BioXFEL center award 1231306 and NIH and Biodesign Center of Advanced Structural Discovery at Arizona State University. We thank Jonah Williams, Brendan Cullinane, Apostolos Zournas and Mathias Miller for constructive discussions.

REFERENCES

(1) Zouni, A.; Witt, H.-T.; Kern, J.; Fromme, P.; Krauss, N.; Saenger, W.; Orth, P. *Nature* **2001**, *409*, 739−743.

(2) Kamiya, N.; Shen, J.-R. *Proc. Natl. Acad. Sci. U. S. A.* **2003**, *100*, 98−103.

(3) Ferreira, K. N.; Iverson, T. M.; Maghlaoui, K.; Barber, J.; Iwata, S. *Science* **2004**, *303*, 1831−1838.

(4) Guskov, A.; Kern, J.; Gabdulkhakov, A.; Broser, M.; Zouni, A.; Saenger, W. *Nat. Struct. Mol. Biol.* **2009**, *16*, 334−342.

(5) Umena, Y.; Kawakami, K.; Shen, J.-R.; Kamiya, N. *Nature* **2011**, *473*, 55−U65.

(6) Petrie, S.; Stranger, R.; Gatt, P.; Pace, R. J. *Chem. - Eur. J.* **2007**, *13*, 5082−5089.

(7) Yano, J.; Kern, J.; Irrgang, K.-D.; Latimer, M. J.; Bergmann, U.; Glatzel, P.; Pushkar, Y.; Biesiadka, J.; Loll, B.; Sauer, K.; et al. *Proc. Natl. Acad. Sci. U. S. A.* **2005**, *102*, 12047−12052.

(8) Davis, K. M.; Pushkar, Y. N. *J. Phys. Chem. B* **2015**, *119*, 3492−3498.

(9) Chapman, H. N.; Fromme, P. *Curr. Opin. Struct. Biol.* **2017**, *45*, 170−177.

(10) Fromme, P. *Nat. Chem. Biol.* **2015**, *11*, 895.

(11) Kupitz, C.; Basu, S.; Grotjohann, I.; Fromme, R.; Zatsepin, N. A.; Rendek, K. N.; Hunter, M. S.; Shoeman, R. L.; White, T. A.; Wang, D.; et al. *Nature* **2014**, *513*, 261−265.

(12) Young, I. D.; Ibrahim, M.; Chatterjee, R.; Gul, S.; Fuller, F. D.; Koroidov, S.; Brewster, A. S.; Tran, R.; Alonso-Mori, R.; Kroll, T.; Michels-Clark, T.; Laksmono, H.; Sierra, R. G.; Stan, C. A.; Hussein, R.; Zhang, M.; Douthit, L.; Kubin, M.; de Lichtenberg, C.; Vo Pham, L.; Nilsson, H.; Cheah, M. H.; Shevela, D.; Saracini, C.; Bean, M. A.; Seuffert, I.; Sokaras, D.; Weng, T.-C.; Pastor, E.; Weninger, C.; Fransson, T.; Lassalle, L.; Bräuer, P.; Aller, P.; Docker, P. T.; Andi, B.; Orville, A. M.; Glownia, J. M.; Nelson, S.; Sikorski, M.; Zhu, D.; Hunter, M. S.; Lane, T. J.; Aquila, A.; Koglin, J. E.; Robinson, J.; Liang, M.; Boutet, S.; Lyubimov, A. Y.; Uervirojnangkoorn, M.; Moriarty, N. W.; Liebschner, D.; Afonine, P. V.; Waterman, D. G.; Evans, G.; Wernet, P.; Dobbek, H.; Weis, W. I.; Brunger, A. T.; Zwart, P. H.; Adams, P. D.; Zouni, A.; Messinger, J.; Bergmann, U.; Sauter, N. K.; Kern, J.; Yachandra, V. K.; Yano, J. *Nature* **2016**, *540*, 453−457.

(13) Kern, J.; Tran, R.; Alonso-Mori, R.; Koroidov, S.; Echols, N.; Hattne, J.; Ibrahim, M.; Gul, S.; Laksmono, H.; Sierra, R. G. *Nat. Commun.* **2014**, *5*, 4371.

(14) Suga, M.; Akita, F.; Hirata, K.; Ueno, G.; Murakami, H.; Nakajima, Y.; Shimizu, T.; Yamashita, K.; Yamamoto, M.; Ago, H.; Shen, J.-R. *Nature* **2015**, *517*, 99−103.

(15) Suga, M.; Akita, F.; Sugahara, M.; Kubo, M.; Nakajima, Y.; Nakane, T.; Yamashita, K.; Umena, Y.; Nakabayashi, M.; Yamane, T.; Nakano, T.; Suzuki, M.; Masuda, T.; Inoue, S.; Kimura, T.; Nomura, T.; Yonekura, S.; Yu, L.-J.; Sakamoto, T.; Motomura, T.; Chen, J.-H.; Kato, Y.; Noguchi, T.; Tono, K.; Joti, Y.; Kameshima, T.; Hatsui, T.; Nango, E.; Tanaka, R.; Naitow, H.; Matsuura, Y.; Yamashita, A.; Yamamoto, M.; Nureki, O.; Yabashi, M.; Ishikawa, T.; Iwata, S.; Shen, J.-R. *Nature* **2017**, *543*, 131−135.

(16) Ayyer, K.; Yefanov, O. M.; Oberthür, D.; Roy-Chowdhury, S.; Galli, L.; Mariani, V.; Basu, S.; Coe, J.; Conrad, C. E.; Fromme, R.; et al. *Nature* **2016**, *530*, 202.

(17) Petrie, S.; Stranger, R.; Pace, R. J. *Phys. Chem. Chem. Phys.* **2017**, *19*, 27682.

DOI: 10.1021/acscatal.8b04513
ACS Catal. 2019, 9, 1396−1407

(18) Tanaka, A.; Fukushima, Y.; Kamiya, N. *J. Am. Chem. Soc.* **2017**, *139*, 1718−1721.
(19) Petrie, S.; Stranger, R.; Pace, R. J. *ChemPhysChem* **2017**, *18*, 2924−2931.
(20) Pushkar, Y.; Jensen, S.; Davis, K. *Biophys. J.* **2018**, *114*, 520a.
(21) Jensen, S. C.; Davis, K. M.; Sullivan, B.; Hartzler, D. A.; Seidler, G. T.; Casa, D. M.; Kasman, E.; Colmer, H. E.; Massie, A. A.; Jackson, T. A.; Pushkar, Y. *J. Phys. Chem. Lett.* **2017**, *8*, 2584−2589.
(22) Kern, J.; Chatterjee, R.; Young, I. D.; Fuller, F. D.; Lassalle, L.; Ibrahim, M.; Gul, S.; Fransson, T.; Brewster, A. S.; Alonso-Mori, R.; Hussein, R.; Zhang, M.; Douthit, L.; de Lichtenberg, C.; Cheah, M. H.; Shevela, D.; Wersig, J.; Seuffert, I.; Sokaras, D.; Pastor, E.; Weninger, C.; Kroll, T.; Sierra, R. G.; Aller, P.; Butryn, A.; Orville, A. M.; Liang, M.; Batyuk, A.; Koglin, J. E.; Carbajo, S.; Boutet, S.; Moriarty, N. W.; Holton, J. M.; Dobbek, H.; Adams, P. D.; Bergmann, U.; Sauter, N. K.; Zouni, A.; Messinger, J.; Yano, J.; Yachandra, V. K. *Nature* **2018**, *563*, 421−425.
(23) Kato, Y.; Akita, F.; Nakajima, Y.; Suga, M.; Umena, Y.; Shen, J.-R.; Noguchi, T. *J. Phys. Chem. Lett.* **2018**, *9*, 2121−2126.
(24) Kupitz, C.; Grotjohann, I.; Conrad, C. E.; Roy-Chowdhury, S.; Fromme, R.; Fromme, P. *Philos. Trans. R. Soc., B* **2014**, *369*, 20130316.
(25) Coe, J.; Kupitz, C.; Basu, S.; Conrad, C. E.; Roy-Chowdhury, S.; Fromme, R.; Fromme, P. *Methods Enzymol.* **2015**, *557*, 459−482.
(26) Ananyev, G.; Carrieri, D.; Dismukes, G. C. *Appl. Environ. Microbiol.* **2008**, *74*, 6102−6113.
(27) Ananyev, G.; Gates, C.; Dismukes, G. C. *Biochim. Biophys. Acta, Bioenerg.* **2016**, *1857*, 1380−1391.
(28) Ananyev, G.; Dismukes, G. C. *Photosynth. Res.* **2005**, *84*, 355−365.
(29) Vinyard, D. J.; Zachary, C. E.; Ananyev, G.; Dismukes, G. C. *Biochim. Biophys. Acta, Bioenerg.* **2013**, *1827*, 861−8.
(30) Ananyev, G.; Gates, C.; Kaplan, A.; Dismukes, G. C. *Biochim. Biophys. Acta, Bioenerg.* **2017**, *1858*, 873−883.
(31) Amin, M.; Askerka, M.; Batista, V. S.; Brudvig, G. W.; Gunner, M. R. *J. Phys. Chem. B* **2017**, *121*, 9382−9388.
(32) Ananyev, G.; Renger, G.; Wacker, U.; Klimov, V. *Photosynth. Res.* **1994**, *41*, 327−338.
(33) Gates, C.; Ananyev, G.; Dismukes, G. C. *Biochim. Biophys. Acta, Bioenerg.* **2016**, *1857*, 1550−1560.
(34) Ishikita, H.; Knapp, E.-W. *J. Am. Chem. Soc.* **2005**, *127*, 14714−14720.
(35) Kato, Y.; Nagao, R.; Noguchi, T. *Proc. Natl. Acad. Sci. U. S. A.* **2016**, *113*, 620−625.
(36) Wiwczar, J.; Brudvig, G. W. In *Photosynthesis: Structures, Mechanisms, and Applications*; Hou, H. J. M., Najafpour, M. M., Moore, G. F., Allakhverdiev, S. I., Eds.; Springer International Publishing: Cham, 2017; pp 51−66.
(37) Petrouleas, V.; Diner, B. A. *Biochim. Biophys. Acta, Bioenerg.* **1987**, *893*, 126−137.
(38) Bao, H.; Zhang, C.; Kawakami, K.; Ren, Y.; Shen, J.-R.; Zhao, J. *Biochim. Biophys. Acta, Bioenerg.* **2008**, *1777*, 1109−1115.
(39) Krivanek, R.; Kern, J.; Zouni, A.; Dau, H.; Haumann, M. *Biochim. Biophys. Acta, Bioenerg.* **2007**, *1767*, 520−527.
(40) Bilger, W.; Schreiber, U.; Bock, M. *Oecologia* **1995**, *102*, 425−432.
(41) Flameling, I. A.; Kromkamp, J. *Limnol. Oceanogr.* **1998**, *43*, 284−297.
(42) Walker, D.; Osmond, C. Measurement of photosynthesis in vivo with a leaf disc electrode: correlations between light dependence of steady-state photosynthetic O2 evolution and chlorophyll a fluorescence transients. *Proceedings of the Royal Society of London. Series B, Biological Sciences* **1986**, *227*, 267−280.
(43) Dau, H.; Zaharieva, I.; Haumann, M. *Curr. Opin. Chem. Biol.* **2012**, *16*, 3−10.
(44) Bendall, D.; Hill, R. *New Phytol.* **1956**, *55*, 206−212.
(45) Kok, B.; Forbush, B.; McGloin, M. *Photochem. Photobiol.* **1970**, *11*, 457−475.
(46) Shinkarev, V. *Biophys. J.* **2005**, *88*, 412−421.
(47) Harbour, J. R.; Bolton, J. R. *Photochem. Photobiol.* **1978**, *28*, 231−234.
(48) Kraljić, I.; Barboy, N.; Leicknam, J.-P. *Photochem. Photobiol.* **1979**, *30*, 631−633.
(49) Shinkarev, V. *Photosynth. Res.* **1996**, *48*, 411−417.
(50) Kurreck, J.; Schödel, R.; Renger, G. *Photosynth. Res.* **2000**, *63*, 171.
(51) Takahashi, Y.; Katoh, S. *Biochim. Biophys. Acta, Bioenerg.* **1986**, *848*, 183−192.
(52) Hakala, M.; Tuominen, I.; Keränen, M.; Tyystjärvi, T.; Tyystjärvi, E. *Biochim. Biophys. Acta, Bioenerg.* **2005**, *1706*, 68−80.
(53) Kroon, B.; Prézelin, B. B.; Schofield, O. *J. Phycol.* **1993**, *29*, 453−462.
(54) Oja, V.; Laisk, A. *Biochim. Biophys. Acta, Bioenerg.* **2000**, *1460*, 291−301.
(55) Babcock, G. T.; Barry, B. A.; Debus, R. J.; Hoganson, C. W.; Atamian, M.; McIntosh, L.; Sithole, I.; Yocum, C. F. *Biochemistry* **1989**, *28*, 9557−9565.
(56) Joliot, P.; Barbieri, G.; Chabaud, R. *Photochem. Photobiol.* **1969**, *10*, 309−329.
(57) de Wijn, R.; van Gorkom, H. J. *Photosynth. Res.* **2002**, *72*, 217−222.
(58) Jee, G.; Koike, H.; Inoue, Y. *Photochem. Photobiol.* **1985**, *42*, 579−585.
(59) Styring, S.; Rutherford, A. W. *Biochim. Biophys. Acta, Bioenerg.* **1988**, *933*, 378−387.
(60) Han, G.; Mamedov, F.; Styring, S. *J. Biol. Chem.* **2012**, *287*, 13422−13429.
(61) Boussac, A.; Rutherford, A. W.; Sugiura, M. *Biochim. Biophys. Acta, Bioenerg.* **2015**, *1847*, 576−586.
(62) Boussac, A.; Rappaport, F.; Carrier, P.; Verbavatz, J.-M.; Gobin, R.; Kirilovsky, D.; Rutherford, A. W.; Sugiura, M. *J. Biol. Chem.* **2004**, *279*, 22809−22819.
(63) Bürgi, H.-B.; Dunitz, J. D. *Structure Correlation*; John Wiley & Sons, Inc.: Hoboken, NJ, 2008.
(64) Elstner, E. F. *Annu. Rev. Plant Physiol.* **1982**, *33*, 73−96.
(65) Semin, B. K.; Davletshina, L. N.; Rubin, A. B. *Photosynth. Res.* **2015**, *125*, 95−103.
(66) Ghanotakis, D. F.; Topper, J. N.; Youcum, C. F. *Biochim. Biophys. Acta, Bioenerg.* **1984**, *767*, 524−531.
(67) Horton, P.; Ruban, A. *Photosynth. Res.* **1992**, *34*, 375−385.
(68) Hanssum, B.; Dohnt, G.; Renger, G. *Biochim. Biophys. Acta, Bioenerg.* **1985**, *806*, 210−220.
(69) Babcock, G. T.; Sauer, K. *Biochim. Biophys. Acta, Bioenerg.* **1975**, *396*, 48−62.
(70) Robinson, H. H.; Crofts, A. R. *FEBS Lett.* **1983**, *153*, 221−226.
(71) de Wijn, R.; van Gorkom, H. J. *Biochemistry* **2001**, *40*, 11912−11922.
(72) Thielen, A.; Van Gorkom, H. *FEBS Lett.* **1981**, *129*, 205−209.
(73) Wraight, C.; Stein, R. In *The Oxygen Evolving System of Photosynthesis*; Elsevier: Amsterdam, 1983; pp 383−392.
(74) Verméglio, A.; Joliot, P. *Biochim. Biophys. Acta, Bioenerg.* **2002**, *1555*, 60−64.

DOI: 10.1021/acscatal.8b04513
ACS Catal. 2019, 9, 1396−1407